Interactions of Lanthanide Complexes with Oxidized Single-Walled Carbon Nanotubes

Tirandai Hemraj-Benny,[†] Sarbajit Banerjee,[†] and Stanislaus S. Wong*[,†,‡]

Department of Chemistry, State University of New York at Stony Brook, Stony Brook, New York 11794-3400, and Materials and Chemical Sciences Department, Brookhaven National Laboratory, Building 480, Upton, New York 11973

Received September 24, 2003. Revised Manuscript Received March 1, 2004

Oxidized, cut single-walled carbon nanotubes (SWNTs) have been reacted with lanthanide salts containing Eu, La, and Tb. These studies are aimed at developing a fundamental understanding of the coordination chemistry of metal ions and of metal ion complexes onto the surfaces of nanotubes. It has been found that the lanthanide ions likely coordinate to these nanotubes through the increased number of oxygen atoms, forming predominantly ionic bonding arrangements. Metal coordination occurs through disruption of hydrogen bonding in bundles of oxidized SWNTs. The adducts were analyzed using FTIR, Raman, and photoluminescence spectroscopies and were structurally characterized using atomic force microscopy (AFM) and transmission electron microscopy (TEM), along with energy-dispersive X-ray spectroscopy (EDS).

Introduction

Single-walled carbon nanotubes (SWNTs) have been the target of intensive interdisciplinary studies because of their unique structure-dependent electronic and mechanical properties.[1−3] The combination of the helicity and diameter of SWNTs, defined by the roll-up vector, determines whether a tube is a metal or a semiconductor. They are thought to have a host of wide-ranging, potential applications including as catalyst supports in heterogeneous catalysis, field emitters, high-strength engineering fibers, sensors, actuators, tips for scanning probe microscopy, gas storage media, and molecular wires for the next generation of electronics devices.[4−8]

Many of these applications require an understanding of the photophysical and electronic properties of these materials. It has been shown that the conductivity properties of SWNTs can be altered by adsorption of molecules that can either donate or accept electrons.[9] In addition, the luminescence properties of SWNTs are affected by the chemical modification of nanotube surfaces with aromatic molecules and polymers.[10,11]

In this work, we have chosen to study complexation of lanthanide ions, Ln^{III}, with oxidized SWNTs, and their effects on nanotube properties. Why lanthanides? Lanthanides, with their large radii and high coordination numbers, as well as unique fluorescence and magnetic properties, have been complexed with semiconducting (conjugated) polymers and organic complexes.[12,13] Applications of these complexes include their use in luminescent sensors and light converters;[14] as nuclear magnetic resonance (NMR) and magnetic resonance imaging (MRI) probes;[15,16] and as practical catalysts in organic and biological reactions.[17] Moreover, previous studies of lanthanide ions, Ln^{III}, with carbon-based nanomaterials have focused on the insertion[18] of lanthanide halides into SWNTs, the encapsulation of lanthanide atoms in endohedral fullerenes,[19] and the trapping of metallofullerenes inside SWNTs.[20] In addition, lanthanides have been incorporated as catalysts

* To whom correspondence should be addressed. Phone: 631-632-1703 or 631-344-3178. Fax: 631-632-7960 or 631-344-4071. E-mail: sswong@notes.cc.sunysb.edu or sswong@bnl.gov.

[†] State University of New York at Stony Brook.

[‡] Brookhaven National Laboratory.

(1) Dresselhaus, M. S.; Dresselhaus, G.; Avouris, P. *Carbon Nanotubes: Synthesis, Structure, Properties, and Applications*; Springer-Verlag: Berlin, 2001.

(2) Falvo, M. R.; Clary, G. J.; Taylor, R. M. I.; Chi, V.; Brooks, F. P. J.; Washburn, S.; Superfine, R. *Nature* **1997**, *389*, 582.

(3) Odom, T. W.; Huang, J.-L.; Kim, P.; Lieber, C. M. *Nature* **1998**, *391*, 62.

(4) Bachtold, A.; Hadley, P.; Nakanshi, T.; Dekker, C. *Science* **2001**, *294*, 1317.

(5) Lordi, V.; Yao, N.; Wei, J. *Chem. Mater.* **2001**, *13*, 733.

(6) Baughman, R. H.; Zakhidov, A. A.; de Heer, W. A. *Science* **2002**, *297*, 787.

(7) Yang, C.-M.; Kanoh, H.; Kaneko, K.; Yudasaka, M.; Iijima, S. *J. Phys. Chem. B* **2002**, *106*, 8994.

(8) Wong, S. S.; Joselevich, E.; Woolley, A. T.; Cheung, C. L.; Lieber, C. M. *Nature* **1998**, *394*, 52.

(9) Kong, J.; Franklin, N. R.; Zhou, C.; Chapline, M. G.; Peng, S.; Cho, K.; Dai, H. *Science* **2000**, *287*, 5453.

(10) Riggs, J. E.; Guo, Z.; Carroll, D. L.; Sun, Y.-P. *J. Am. Chem. Soc.* **2000**, *122*, 5879.

(11) Qu, L.; Martin, R. B.; Huang, W.; Fu, K.; Zweifel, D.; Lin, Y.; Sun, Y.-P. *J. Chem. Phys.* **2002**, *117*, 8089.

(12) McGehee, M. D.; Bergstedt, T.; Zhang, C.; Saab, A. P.; O'Regan, M. B.; Bazan, G. C.; Srdanov, V. I.; Heeger, A. J. *Adv. Mater* **1999**, *11*, 1349.

(13) Wan, Y.; Zhang, L.; Jin, L.; Gao, S.; Lu, S. *Inorg. Chem.* **2003**, *42*, 4985.

(14) Parker, D. *Coord. Chem. Rev.* **2000**, *205*, 109.

(15) Parker, D. *Chem. Rev.* **1991**, *91*, 1441.

(16) Caravan, P.; Ellison, J. J.; McMurry, T. J.; Lauffer, R. B. *Chem. Rev.* **1999**, *99*, 2293.

(17) Komiyama, M.; Takeda, N.; Shigekawa, H. *Chem. Commun.* **1999**, 1443.

(18) Xu, C.; Sloan, J.; Brown, G.; Bailey, S.; Williams, V. C.; Friedrichs, S.; Coleman, K. S.; Flahaut, E.; Hutchison, J. L.; Dunin-Borkowski, R. E.; Green, M. L. H. *Chem. Commun.* **2000**, 2427.

(19) Ding, J.; Yang, S. *J. Phys. Chem. Solids* **1997**, *58*, 1661.

(20) Smith, B. W.; Luzzi, D. E.; Achiba, Y. *Chem. Phys. Lett.* **2000**, *331*, 137.

10.1021/cm0349147 CCC: $27.50
Published on Web 04/09/2004

used in the production of carbon nanotubes.[21,22] To the best of our knowledge, the interactions of simple lanthanide, Ln^{III}, salts with the surfaces of SWNTs have not been studied. Moreover, this current work is an extension of the efforts[23−27] of our group in understanding metal complexation onto nanotubes as a means of enhancing and understanding nanotube solubilization, catalysis, charge transfer, separation, and processability. In addition, it builds upon the work of other groups in creating novel nanoscale interconnects[28] and forest assemblies[29] based on coordinative nanotube−metal interactions.

As such, in this study, we analyze the complexation of chloride and nitrate salts of europium (Eu^{3+}), terbium (Tb^{3+}), and lanthanum (La^{3+}) with purified, oxidized, cut SWNTs, functionalized with carboxy and alcohol groups. In independent runs, hydrated lanthanum(III) chloride hydrated ($LaCl_3 \cdot xH_2O$); lanthanum(III) nitrate hexahydrate ($La(NO_3)_3 \cdot 6H_2O$); anhydrous europium(III) chloride ($EuCl_3$); europium(III) nitrate hexahydrate ($Eu(NO_3)_3 \cdot 6H_2O$); terbium(III) chloride hexahydrate ($TbCl_3 \cdot 6H_2O$); and terbium(III) nitrate hexahydrate ($Tb(NO_3)_3 \cdot 6H_2O$) were added to our processed tubes. Functionalized adducts were studied by atomic force microscopy (AFM), transmission electron microscopy (TEM), and energy-dispersive X-ray spectroscopy (EDS) as well as by Raman, Fourier transform infrared (FTIR), and photoluminescence spectroscopies.

Experimental Section

Processing of Purified, Cut Tubes. Raw Carbolex SWNTs (Figure 1a) were purified according to modifications of existing purification protocols.[30,31] Specifically, a sample of raw SWNTs was initially ultrasonicated in 2.6 M HNO_3 for ∼10 min to disperse the solid tubes. The reaction mixture was subsequently refluxed for 40 h. The black mixture was cooled to room temperature and filtered using a 0.2-μm polycarbonate membrane. As reported, this initial oxidation step results in a 70−80% weight loss, during which most of the carbonaceous impurities and metallic particles are removed.[5] To eliminate remaining carbonaceous impurities without further destroying the SWNTs, the tubes were refluxed in distilled water for 1 h. The mixture was then filtered over a 0.2-μm polycarbonate membrane and dried at 100 °C. An AFM image of the purified product (Figure 1b), corroborated by TEM results, verifies the efficacy of impurity removal from the tube surface. SWNT bundles ranging between 15 and 50 nm wide were observed. As a result of this initial oxidation step, a significant density of oxygenated functional groups is introduced on the end caps and defect sites.

Cut tubes were prepared in a three-step process consisting of cutting, polishing, and washing.[30,32] Typically, a sample of purified SWNTs was cut by sonication in a 3:1 H_2SO_4/HNO_3 mixture for 20 min. After filtration, it was further sonicated in distilled water for 30 min and then filtered over a polycarbonate membrane with sufficient washing with water until the filtrate pH attained ∼7. The sample was then dried at 100 °C for 30 min. "Polishing"[30,32] was performed by stirring the sample in an aqueous 4:1 H_2SO_4/30% aq H_2O_2 mixture for 30 min. After further dilution, filtration, and drying, the final processing step involved washing of the tubes with a 1:1 HCl/H_2O mixture to ensure that the opened ends of the purified SWNTs were terminated with carboxylic acid groups rather than with carboxylate groups. A TEM image (Figure 1c) of cut tubes showed bundles, ranging from ∼2 to 25 nm wide and 100 to 300 nm long. EDS data (inset to Figure 1c) indicated the presence of oxygenated groups, which are expected to include carboxylic acid and alcohol groups, based on independent XPS studies. These oxygenated groups are found on the surface of oxidized SWNTs, particularly at defect sites.[33] Although some amount of residual nickel catalyst was detected, there were no signals attributed to lanthanide ions.

Synthesis of Oxidized SWNT−Ln^{III} Complex Adducts. Established procedures for generating metal-complex-functionalized nanotubes were followed.[23−25] A typical reaction was carried out using a Schlenk setup under nitrogen atmosphere. Initially, a sample of shortened, oxidized SWNTs (∼2 mg) was briefly sonicated in dimethylformamide (DMF) to disperse the solid tubes in solution, which was then vigorously stirred. A 0.01 M solution of either a Eu, La, or Tb salt (nitrate or chloride) in DMF was then added dropwise to the purified, oxidized, cut SWNTs. The mixture was subsequently stirred at room temperature for a period of 90 h. From our prior experience with performing a number of similar nanotube reactions,[23,24] longer reaction times are often helpful to maximize diffusion of reactants into bundles, as the nanotubes are found as dispersions and not as true solutions. However, immediately upon mixing, many oxygenated surface sites will and do become functionalized. Thus, long reaction times are not a necessary condition for functionalization. Upon filtration over a 0.2-μm polycarbonate membrane, the solid SWNTs were washed several times with DMF. The resulting solid was vacuum-dried for ∼24 h. TEM images and EDS data were obtained for all of the adducts (Figure 2).

Atomic Force Microscopy. AFM height images were taken in tapping mode in air at resonant frequencies of 50−75 kHz with oscillating amplitudes of 10 to 100 nm. The samples were spin coated onto a mica substrate, and imaged with Si tips ($k = 1-5$ N/m) using a Multimode Nanoscope IIIa (Digital Instruments, Santa Barbara, CA).

Transmission Electron Microscopy. TEM samples were obtained by drying sample droplets from an ethanolic dispersion onto a 300-mesh Cu grid coated with a lacey carbon film. All the micrographs were taken at an accelerating voltage of 120 kV on a Philips CM 12 TEM, equipped with EDS capabilities.

Spectroscopy. FTIR data were obtained on a Nexus 670 (Thermo Nicolet) equipped with a single reflectance ZnSe ATR accessory, a KBr beam splitter, and a DTGS KBr detector. Samples were placed on a ZnSe crystal. Data were taken with a reproducible pressure.

FT Raman spectra were obtained on a Brüker instrument on dispersions of the functionalized nanotubes in DMF. The Raman data were acquired, after 100−200 scans, upon excitation of a 1064-nm Nd:YAG laser, using a liquid-N_2-cooled Ge detector. For Raman microprobe measurements, samples were drop cast onto Si wafers and spectra were collected at 632.8-nm excitation on a Kaiser Raman microscope.

Fluorescence data were obtained at 25 °C on a Jobin Yvon Spex Fluorolog 3. Data were taken with a 1-s integration time.

(21) Kiang, C. H.; Goddard, W. A.; Beyers, R.; Bethune, D. S. *Carbon* **1995**, *33*, 903.
(22) Shi, Z.; Ozakazi, T.; Shimada, T.; Sugai, T.; Suenaga, K.; Shinohara, H. *J. Phys. Chem. B* **2003**, *107*, 2485.
(23) Banerjee, S.; Wong, S. S. *Nano Lett.* **2002**, *2*, 49.
(24) Banerjee, S.; Wong, S. S. *J. Am. Chem. Soc.* **2002**, *124*, 8940.
(25) Banerjee, S.; Kahn, M. G. C.; Wong, S. S. *Chem. Eur. J.* **2003**, *9*, 1898.
(26) Banerjee, S.; Wong, S. S. *Adv. Mater.* **2004**, *16*, 34.
(27) Banerjee, S.; Wong, S. S. *J. Am. Chem. Soc.* **2004**, *126*, 2073.
(28) Frehill, F.; Vos, J. G.; Benrezzak, S.; Koos, A. A.; Konya, Z.; Ruther, M. G.; Blau, W. J.; Fonseca, A.; Nagy, J. B.; Biro, L. P.; Minett, A. I.; in Het Panhuis, M. *J. Am. Chem. Soc.* **2002**, *124*, 13694.
(29) Chattopadhyay, D.; Galeska, I.; Papadimitrakopoulos, F. *J. Am. Chem. Soc.* **2001**, *123*, 9451.
(30) Liu, J.; Rinzler, A. G.; Dai, H.; Hafner, J. H.; Bradley, R. K.; Boul, P. J.; Lu, A.; Iverson, T.; Shelimov, K.; Huffman, C. B.; Rodriguez-Macias, F.; Shon, Y. S.; Lee, T. R.; Colbert, D. T.; Smalley, R. E. *Science* **1998**, *280*, 1253.
(31) Chiang, I. W.; Brinson, B. E.; Smalley, R. E.; Margrave, J. L.; Hauge, R. H. *J. Phys. Chem. B* **2001**, *105*, 1157.
(32) Chen, J.; Hamon, M. A.; Hu, H.; Chen, Y.; Rao, A. M.; Eklund, P. C.; Haddon, R. C. *Science* **1998**, *282*, 95.
(33) Hiura, H.; Ebbesen, T. W.; Tanigaki, K. *Adv. Mater.* **1995**, *7*, 275.

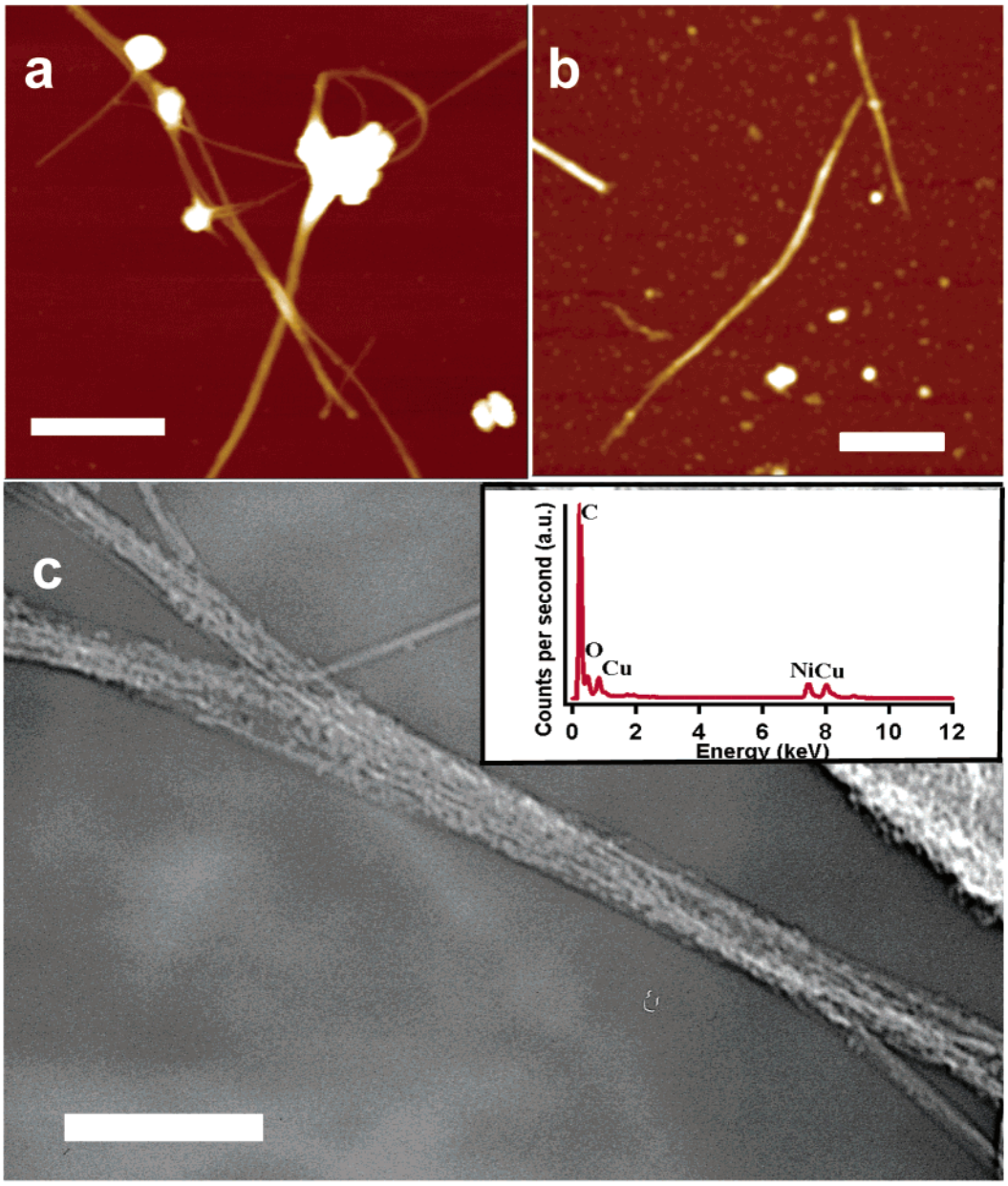

Figure 1. AFM height images of (a) as-prepared Carbolex SWNTs and (b) oxidized SWNTs. Scale bars are 250 nm in both cases. (c). TEM image of shortened, oxidized SWNTs. Scale bar is 50 nm. Inset represents EDS spectrum of oxidized, shortened SWNTs. Cu signal originates from the grid used in the sample preparation.

PL spectra for Eu^{3+} and Tb^{3+} were obtained at excitation wavelengths of 394 and 340 nm, respectively. The interaction of dried, oxidized, cut SWNTs with $TbCl_3$ and $EuCl_3$ complexes in anhydrous DMF was followed at successive time intervals. Specifically, 1 mg of the dried, oxidized, cut SWNTs was added to 0.01 M $EuCl_3$ solution in anhydrous DMF, which was then sonicated for approximately 10 s to obtain a visually nonscattering dispersion of SWNTs. Fluorescence data were taken immediately afterward ($t = 0$ min) and again at subsequent time intervals without any additional sonication or stirring steps. An identical procedure was repeated using the $TbCl_3$ analogue.

Results and Discussion

Microscopy Confirmation of Adduct Formation. Figure 2 shows the TEM images and the corresponding EDS data of the SWNT adducts composed of the chloride salts of Eu^{3+}, Tb^{3+}, and La^{3+}. Similar data were obtained for SWNT adducts formed from the corresponding nitrate salts. A small degree of exfoliation in the oxidized SWNT bundles was observed upon functionalization. Bundles of ~5 nm wide were the predominant motif for the Tb^{3+}- and La^{3+}-derivatized nanotube adducts. For the Eu^{3+}-functionalized adducts, slightly larger bundles of ~20 nm wide were also observed, though very small bundles and even single tubes of ~1 nm diameter were also noted. With each adduct, the presence of the expected metal in the adduct structure was confirmed by EDS spectra, as shown in Figure 2. Considering the functionalized SWNTs adducts were thoroughly washed with DMF to remove any extraneous, unbound metal salt, it can be reasonably assumed that the metal ions presently observed were coordinated onto the SWNTs. It is noteworthy that EDS is consistent with the presence of lanthanide ions localized on the nanotube surface. However, only spectroscopic studies as discussed in subsequent sections can conclusively

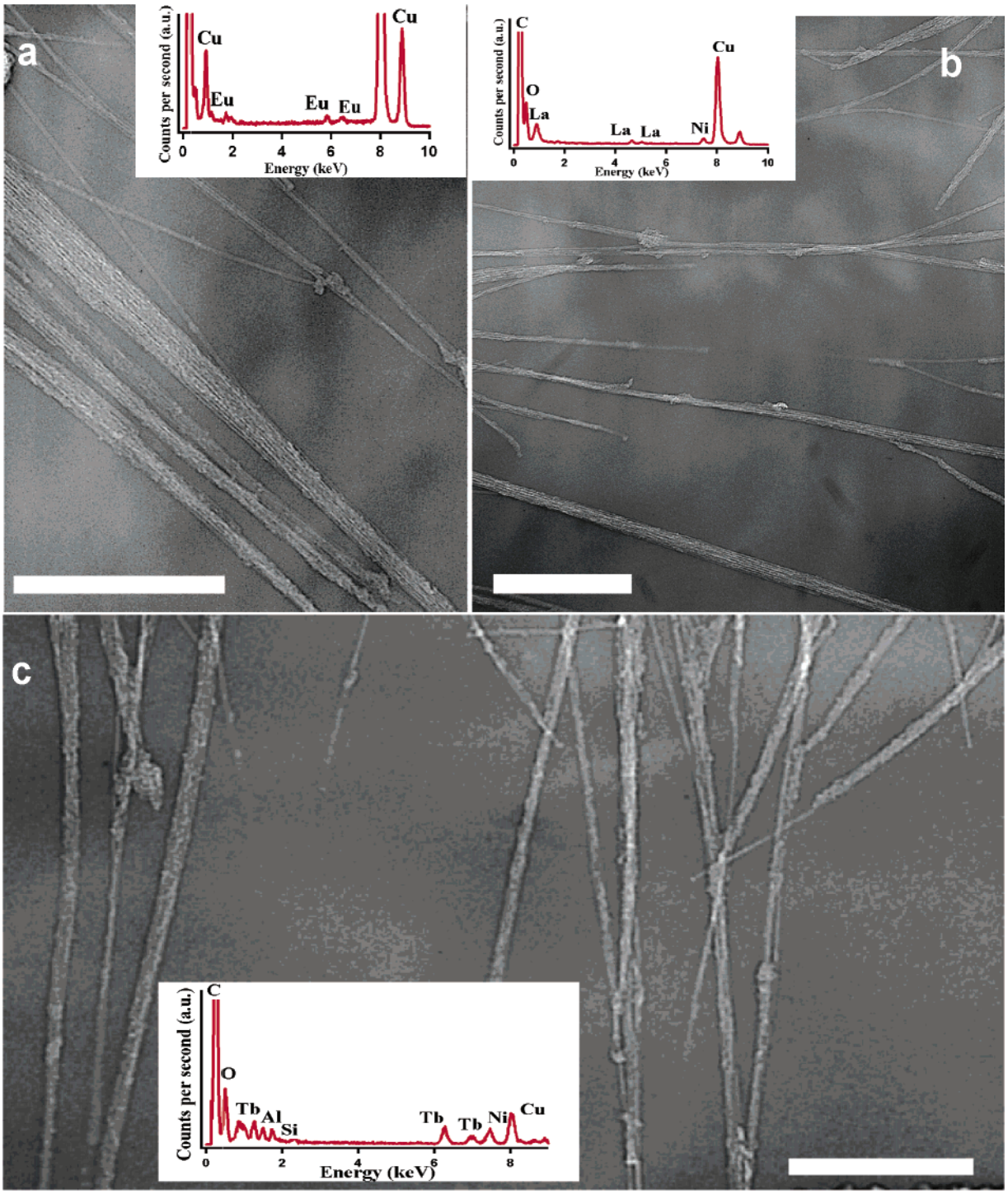

Figure 2. TEM images of (a) Eu^{3+}−SWNT adducts, (b) La^{3+}−SWNTs adducts, and (c) Tb^{3+}−SWNT adducts formed from the lanthanide chloride salts. All scale bars are 100 nm. Insets in corresponding images represent EDS data of respective Ln^{3+}−SWNTs adducts. Cu signal originates from the grid used in the sample preparation. In addition, it should be noted that the small amounts of Al and Si detected may come from etching of the glass reaction flask by nitric acid during the purification and oxidation steps.[68] These impurities are not closely associated with the nanotubes themselves, and, moreover, are not expected to have any bearing on the complexation of the lanthanide ions to the nanotubes.

elucidate the nature of the metal ion−nanotube interaction.

Infrared Data Interpretation: Hydrogen Bonding, Coordination Modes, and Ionic Interactions in Adducts. The presence of IR peaks in the oxidized tubes is associated with the oxygenated functionalities as opposed to the nanotubes themselves, which have few IR-active modes in their pristine form, due to their high intrinsic symmetry. The spectra (in Figures 3a and 4a) of our initial, oxidized, and shortened SWNTs consisted of four major peaks, which were downshifted compared with the nanotube literature values.[34,35] The main peak at 1693 cm^{-1} is assigned to the −C═O stretching vibration in the COOH group. This was a downshift of

(34) Zhang, J.; Zou, H.; Quing, Q.; Yang, Y.; Li, Q.; Liu, Z.; Guo, X.; Du, Z. *J. Phys. Chem. B* **2003**, *107*, 3712.
(35) Kuznetsova, A.; Mawhinney, D. B.; Naumenko, V.; Yates, J. T., Jr; Liu, J.; Smalley, R. E. *Chem. Phys. Lett.* **2000**, *321*, 292.

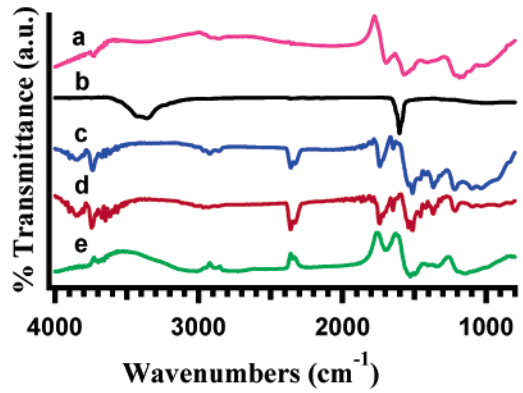

Figure 3. Mid-IR data of Ln^{3+}−SWNT adducts obtained from the respective lanthanide chlorides. Top to bottom: (a) oxidized, shortened SWNTs (pink); (b) Eu^{3+} chloride salts typical of all lanthanide chloride salts studied (black); (c) Eu^{3+}−SWNT adducts (blue); (d) Tb^{3+}−SWNT adducts (red); and (e) La^{3+}−SWNT adducts (green).

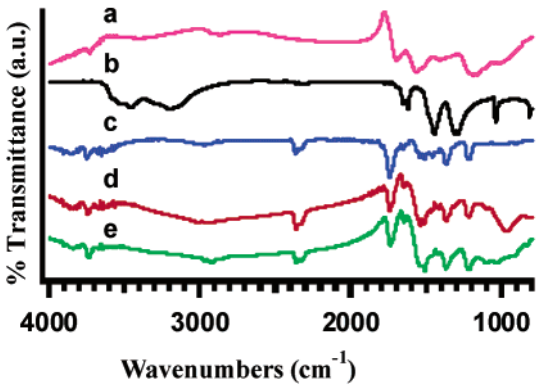

Figure 4. Mid-IR data of Ln^{3+}−SWNT adducts obtained from the respective lanthanide nitrates. Top to bottom: (a) oxidized, shortened SWNTs (pink); (b) Eu^{3+} nitrate salts typical of all lanthanide salts studied (black); (c) Eu^{3+}−SWNT adducts (blue); (d) Tb^{3+}−SWNT adducts (red); and (e) La^{3+}−SWNT adducts (green).

42 cm^{-1}, which can be interpreted as due to an increase in hydrogen bond formation between adjacent −COOH groups. That is, hydrogen bonding causes the observed frequency to decrease due to a lessening in the degree of double bond character in the −COOH group.[34,36] The exact magnitude of the observed downshift associated with hydrogen bonding depends on the packing arrangements of the oxidized tubes, which in turn are affected by a number of factors including the degree of tube oxidation and defect site density as well as the lengths, sizes, and number of tubes within the nanotube ropes. Hydrogen bonding between carboxyl groups attached on the ends and sidewalls of oxidized SWNTs, for example, has been found to contribute to the stacking behavior of these tubes into larger bundles and networks.[37,38]

The ν(C−O) stretch, reported in the literature at ∼1245 cm^{-1}, was noted at 1185 cm^{-1} in our system, which could also be ascribed to hydrogen bonding. A C=C− peak at 1566 cm^{-1} could be attributed to the carbon skeleton in-plane E_{1u} stretch of the nanotube. Although there is some speculation as to the origin of the 1408 cm^{-1} peak, it may be due to an O−H bending vibration.[39]

To re-emphasize, the likely presence of hydrogen bonding is an indicator of nonionized −COOH groups as opposed to $-COO^-$ groups in the starting material. Further evidence for the existence of hydrogen bonding comes from the relatively facile dispersability of oxidized tubes in H_2O as compared with pristine, raw tubes, as well as the corresponding difficulty in dispersing these oxidized tubes in nonpolar CS_2. This is an important point because it implies that the starting oxidized, cut tubes were likely free of potentially interfering, coordinated metal ions prior to the derivatization experiment. Hence, by studying the change in frequency of the protonated carboxyl group in the nanotube adduct, upon addition of the lanthanide salts to the nanotubes, one can determine the type of coordination between the metal ion and the SWNTs.[36,40,41]

All of the starting lanthanide chloride and nitrate salt reagents yielded water bending vibrations (H−O−H) between 1602 and 1653 cm^{-1} (Figures 3b and 4b),[42] which were not observed in the spectrum of the lanthanide metal-derivatized SWNT adducts (Figures 3c, d and e and 4c, d and e). Moreover, −O−H stretches from water, observed above 3000 cm^{-1}, which were detected for all of the chloride and nitrate lanthanide salts, were no longer visible in the adducts. In addition, the nitrate salts possessed NO_2 anti-symmetric stretches between 1435 and 1448 cm^{-1} and NO_2 symmetric stretches between 1294 and 1312 cm^{-1}, which were not subsequently noted in the IR spectra of the corresponding functionalized adducts (Figure 4c and d). These data further support the efficacy of vacuum-drying as well as of removing remaining, unbound metal salt complex from the resultant derivatized SWNTs. As a result, it can be safely assumed that coordination occurred mainly between the metal ions and the SWNTs. The presence of chloride or nitrate ions was relatively insignificant.

From Figures 3 and 4 there were no notable spectroscopic differences observed between derivatized SWNT adducts obtained from either the nitrate or the chloride salts of europium and terbium. The IR spectra of the lanthanum nitrate salt complex-derivatized SWNT adducts (Figure 4e) correlated well with that of the corresponding europium- and terbium-derivatized SWNT analogues (Figure 4c and d). There were, however, clear variations noted for the lanthanum chloride salt-derivatized SWNT adduct (Figure 3e) as compared with the chloride analogues (Figure 3c and d) of the other two lanthanides. These will be discussed later.

For the sake of simplicity, the infrared characteristics of only the europium(III) chloride-derivatized SWNT adduct (Figure 3c) will be described. A similar discussion can be made for all of the other adducts, except for that derived from lanthanum(III) chloride. Generally, nonionized and noncoordinated carbonyl stretching bands

(36) Sawyer, D. T.; Paulsen, P. J. *Alkaline Earth Chelates* **1957**, *80*, 1597.
(37) Kukovecz, A.; Kramberger, C.; Holzinger, M.; Kuzmany, H.; Schalko, J.; Mannsberger, M.; Hirsch, A. *J. Phys. Chem. B* **2002**, *106*, 6374.
(38) Kovtyukhova, N. I.; Mallouk, T. E.; Pan, L.; Dickey, E. C. *J. Am. Chem. Soc.* **2003**, *125*, 9761.
(39) Dragan, S.; Fitch, S. *J. Chem. Educ.* **1998**, *75*, 1018.
(40) Duckworth, O. W.; Martin, S. T. *Geochim. Cosmo. Acta* **2001**, *65*, 4289.
(41) Dioumaev, A. K. *Biochemistry (Moscow)* **2001**, *66*, 1269.
(42) Taylor, M. D.; Cheung, T. T.; Hussein, M. A. *J. Inorg. Nucl. Chem.* **1972**, *34*, 3073.

occur at 1750−1700 cm^{-1},[39] the analogues of which were noted at 1739 cm^{-1} in our nanotube adducts. One explanation for the observed upshift from 1693 cm^{-1} is the decrease in hydrogen bonding, and hence, the consequent increase in double bond character of the C═O group in our adducts. The C−O stretching vibration of the oxidized SWNTs at 1185 cm^{-1} is also believed to have upshifted to 1219 cm^{-1} due to the reduction of hydrogen bonding. We believe that this overall reduction of hydrogen bonding is a result of coordination of the metal ions to the oxygenated groups on the SWNTs. That is, as a result, the oxygenated functional groups that have attached to the metal ions are no longer capable of simultaneously participating in hydrogen bonding with their neighboring moieties. Hence, one consequence of functionalization, confirmed by TEM (Figure 2) as well as by Raman data, which are to be discussed later, is that the larger bundles exfoliate to smaller ones upon derivatization with lanthanides. This is also in agreement with observations in Rh-based systems.[24]

From infrared data, we also have insight into the nature of the metal complex−SWNT bond formation. Bound, deprotonated carboxylate groups, $-COO^-$, display an antisymmetric vibration at 1550−1610 cm^{-1} and a symmetric vibration at 1300−1420 cm^{-1}.[41] In our adducts, the 1368 cm^{-1} peak can be associated with the symmetric carbonyl vibration of the coordinated groups, while the 1644, 1537, and 1513 cm^{-1} bands can be correlated with the antisymmetric vibrations of variously coordinated metal−carbonyl bonds. Considering the downshift of the carbonyl peaks expected at 1693 cm^{-1}, it is plausible that the type of bonding between the metal ions and the oxygenated groups on the SWNTs is predominantly ionic. With ionic bonding there is an increased possibility for carboxylate resonance, which enhances the single-bond character of the carbonyl group, and thus, lowers the frequency of the C═O stretching vibration.

How might this coordination occur? It is expected, on the basis of previously reported carboxylate metal coordination studies,[40] that there are different modes of coordination occurring between the lanthanide metal ions and the oxygenated groups on the nanotube. One or both oxygen atoms of the oxygenated carboxylate moiety can interact with the metal atoms. If we define $\Delta\nu$ as the spectral separation between symmetric and asymmetric stretches of the surface carboxylate groups, values of $\Delta\nu > 200$ cm^{-1} are indicative of a single bond between the metal and the carboxylate group, whereas values of $\Delta\nu < 150$ cm^{-1} suggest a bidentate, bridging, twice-bonded structure.[40] That is, the spectral separation upon complexation increases because of the reduction in group symmetry, thereby broadening the difference between the strength of the carbon−oxygen oscillators. Hence, the peak at 1644 cm^{-1} (corresponding to a $\Delta\nu$ of 276 cm^{-1}) for the nanotube adduct likely represents single coordination, whereas the 1537 and 1513 cm^{-1} peaks, corresponding to $\Delta\nu$ values of 169 and 145 cm^{-1}, are likely associated with twice-bonded or bridging coordination. On the basis of this analysis, possible coordination modes of lanthanide metal ions with the oxygenated groups on the nanotube are shown in Figure 5.

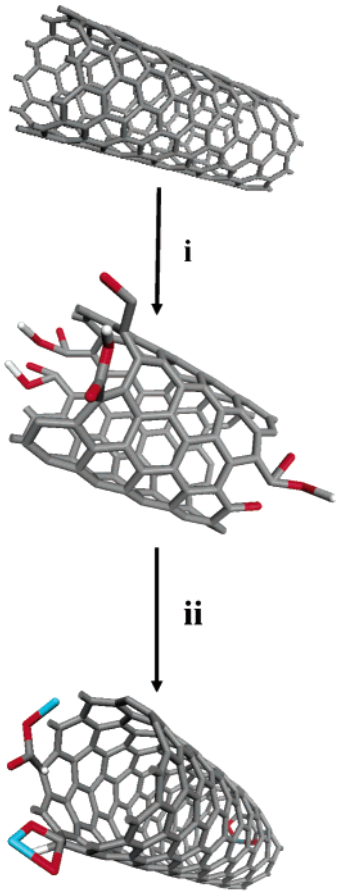

Figure 5. Schematic of proposed forms of attachment of lanthanide ions to SWNTs. Step (i): raw, pristine tubes are oxidized with nitric acid; result is a decoration of the ends of SWNTs with oxygenated groups. Step (ii): functionalization of oxidized nanotubes with Ln^{3+} salts. Single-bonded and twice-bonded metal coordination, respectively, with Ln^{3+} ions onto SWNTs are depicted. Color scheme: white, hydrogen; red, oxygen; and blue, Ln^{3+}.

As previously discussed and from Figure 3, the infrared spectrum of the SWNT adduct derived from lanthanum (III) chloride differed from that of the other lanthanide salt complexes studied. It was concluded that the La metal ion likely did not coordinate with the SWNTs in the same manner as the others, since the C═O stretching vibrational peak at 1694 cm^{-1} remained relatively unchanged upon adduct formation, implying that there was no significant decrease in hydrogen bonding. Moreover, there was no evidence of single bond coordination, as no 1650 cm^{-1} peak, characteristic of such a band, was observed. Nonetheless, there were peaks at lower wavenumbers, suggestive of the possibility of bridging, bidentate interactions occurring between the metal ion and the oxygenated groups. The reason for the different mode of coordination observed with lanthanum chloride, as compared with the other lanthanides, is not yet understood.

Photoluminescence Results: Nanotube Quenching of Lanthanide Fluorescence. Photoluminescence (PL) spectroscopy provides an opportunity to study specific chemical interactions of various reactive ligands (such as carbon nanotubes) with lanthanide ions (such as Eu^{3+} and Tb^{3+}). These lanthanide ions possess particularly good luminescent properties based on electronic transitions between 4*f* energy levels. These

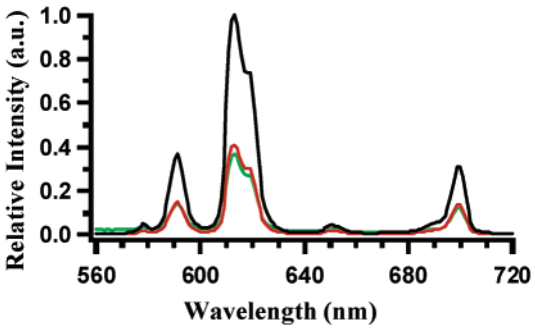

Figure 6. Photoluminescence data on Eu^{3+}−SWNT complexes. The interaction of dried SWNTs with lanthanide complexes in anhydrous DMF was analyzed at consecutive time intervals. Top to bottom: 0.01 M $EuCl_3$ in DMF (black); 1 mg of SWNTs added to 0.01 M $EuCl_3$ salt in DMF (red) (t = 0 min); and 1 mg of SWNTs added to 0.01 M $EuCl_3$ salt in DMF (green) (t = 5 min).

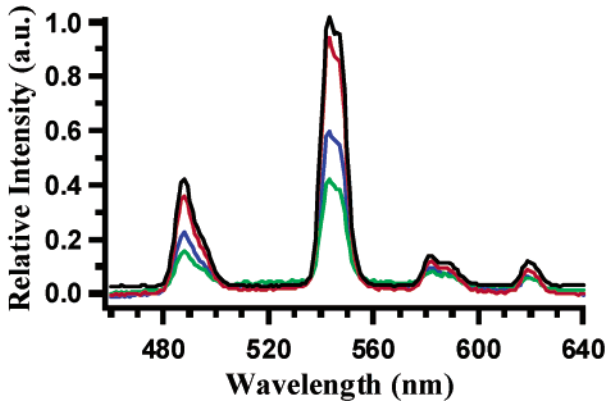

Figure 7. Photoluminescence data on Tb^{3+}−SWNT complexes. Top to bottom.: 0.01 M $TbCl_3$ in DMF (black); 1 mg of SWNTs added to 0.01 M $TbCl_3$ salt in DMF (red) (t = 0 min); 1 mg of SWNTs added to 0.01 M $TbCl_3$ salt in DMF (blue) (t = 5 min); and 1 mg of SWNTs added to 0.01 M $TbCl_3$ salt in DMF (green) (t = 10 min).

transitions are dependent primarily on the nature of the metal ion. In effect, upon excitation of free Ln^{III} ions, energy relaxation from the ^5D to ^7F states occurs and results in a sharp emission at specific wavelengths. In studying the Eu^{III} and Tb^{III} luminescence spectra (Figures 6 and 7, respectively), significant quenching was observed upon addition of purified, shortened, oxidized SWNTs. Similar measurements with La^{3+} were not possible as these ions do not strongly fluoresce. The specific lanthanide transitions observed in the figures are consistent with reports in the literature.[43] It is relevant to point out that pristine tubes do not disperse in the solvents necessary for PL measurements of interactions of these tubes with lanthanide complexes.

It is believed that SWNTs can serve as electron acceptors,[44−46] and hence, can act as an energy sink in an excited-state energy transfer mechanism. Indeed, upon coordination of these Ln^{III} ions to the oxidized SWNTs, and subsequently upon relaxation after excitation, some degree of energy transfer is expected from the metal to the low-lying excited states in the visible and near-IR regions of the SWNTs, which thereby results in a decreased intensity in the intrinsic emission of the Ln^{III} ions. Hence, upon initial addition of nanotubes to the lanthanide solution, the lanthanide PL is quenched as the lanthanide ions complex to the surface. It is important to note that although water is known to quench Ln^{III} emission, its presence is unlikely to be the reason for the observed quenching in our dried, oxidized SWNT adducts, measured in DMF, as no additional source of hydration was introduced into the system probed.

Photoluminescence studies were performed for a duration of up to ∼1 h after the oxidized, cut nanotubes were initially mixed with lanthanide salts, due to ensuing changes in the nature of the sample (in an unstirred and unsonicated environment) that we later describe. As mentioned, initially, within minutes, the fluorescence of lanthanide ions is quenched when these species are localized on the nanotube. At a significantly later point in time though, the fluorescence intensity increases. This can be attributed to changes in the nature of the sample due to the cut, oxidized SWNTs crashing out of the DMF and accompanying regeneration of solvated lanthanide ions. How can this be plausibly explained?

Mechanistically, the nanotube−lanthanide ion interaction involves a rapid exchange of lanthanide ions freely circulating in solution and of lanthanide ions bound to the nanotubes. In other words, lanthanide ions are easily migrating onto and off the nanotube surface. The key is that the rate of this migration/exchange process will likely be very different depending on whether the nanotube is suspended in solution or whether the nanotube has crashed out of solution. In other words, the change in exchange kinetics accounts for the observed variation in PL intensity, as the nanotubes crash out and the relative concentration of free lanthanide ions increases. Moreover, when nanotubes crash out, the tubes essentially start to bundle together into larger ropes held together by nonspecific interactions such as van der Waals forces and hydrogen bonding. This can result in certain nanotube sites becoming unavailable for lanthanide complexation. It is worth reiterating that no stirring or sonication was performed after starting the PL experiment, so potential tube aggregation during the data collection process was not reversed, unlike for the actual reaction itself, where vigorous stirring was maintained to obtain better diffusion of the reactants. Thus, overall, as fewer lanthanide ions remain coordinated to the nanotube, the PL intensity of the unbound lanthanide ions understandably starts to increase again.

Our results are also in agreement with the weakened photoluminescence observed in alkylthio-group-substituted phthalocyanine rare-earth sandwich complexes,[47] the quenching of pyrene fluorescence by tethered nanotubes,[11] and the reported reduction in stilbene emission intensities when coupled to nanotubes.[48] Notably, as aggregate bundles as opposed to individualized SWNTs

(43) Liu, P.; Liang, D.; Tong, Z.; Liu, X. *Macromolecules* **2002**, *35*, 1487.
(44) Ago, H.; Shaffer, M. S. P.; Ginger, D. S. *Phys. Rev. B* **2000**, *61*, 2286.
(45) Cao, L.; Chen, H. Z.; Zhou, H. B.; Zhu, L.; Sun, J. Z.; Zhang, X. B.; Xu, J. M.; Wang, M. *Adv. Mater.* **2003**, *15*, 909.
(46) Romero, D. B.; Carrard, M.; Zuppiroli, L. *Adv. Mater.* **1996**, *8*, 899.
(47) Yoshino, K.; Lee, S. B.; Sonoda, T.; Kawagishi, H.; Hidayat, R.; Kakayama, K.; Ozaki, M.; Ban, K.; Nishizawa, K.; Ohta, K.; Shirai, H. *J. Appl. Phys.* **2000**, *88*, 7137.

were analyzed, the band gap luminescence of semiconducting tubes is expected to be quenched by the presence of metallic tubes. Thus, we were unable to observe any noticeable band gap emission in these studies. Emission from defective, oxidized tubes is expected to be weak and to be likely overwhelmed by that of the lanthanide ions themselves.

As suggested by the IR data, the coordination between the Ln^{III} ions and the oxidized SWNTs occurs primarily through ionic type bonding and not through covalent interaction. This observation is further emphasized by the luminescence data. In general, shifts of emission bands to longer wavelengths upon complexation suggest the presence of covalent interactions.[49] However, in our particular experiment, this was not observed for either the Eu^{III} or the Tb^{III} ions upon derivatization with SWNTs, thereby strengthening the argument for ionic interaction.

Raman Data: Evidence for Disruption of Hydrogen Bonding and Acid Deintercalation from Oxidized Nanotube Bundles Upon Lanthanide Functionalization. Raman spectroscopy is a particularly sensitive probe of electronic and vibrational structure and their coupling in SWNTs.[50] Raman spectra are resonance-enhanced at selected laser excitation wavelengths due to coupling with the optically allowed electronic transitions between the van Hove singularities in the electronic density of states of the SWNTs. The radial breathing modes (RBM) near 200 cm^{-1} correspond to symmetric, in-phase motion of carbon atoms perpendicular to the nanotube axis and depend sensitively on tube diameter.[51] The high-frequency G modes[52] near ~1590 cm^{-1} and the second-order G′ bands[53] near 2600 cm^{-1}, related to tangential C−C stretching modes of graphite, are sensitive to the charge exchanged between nanotubes and guest atoms that have intercalated into the interstitial channels in the tube bundles. The shape and intensity of a weak disorder mode peak, originating from defects in the curved graphene sheets and tube ends, at 1290−1320 cm^{-1} has also been correlated with the extent of nanotube sidewall functionalization.[54]

RBM modes are related to the diameter of SWNTs, as in eq 1:[55]

$$\omega_R = [223.75 \text{ nm cm}^{-1}/d \text{ (nm)}] + 14 \text{ cm}^{-1} \quad (1)$$

Different subsets of tubes are brought into resonance by selected laser excitation energies.[50] The RBM features observed at a particular laser excitation energy thus depend on the diameter of the nanotubes that are brought into resonance at that energy.

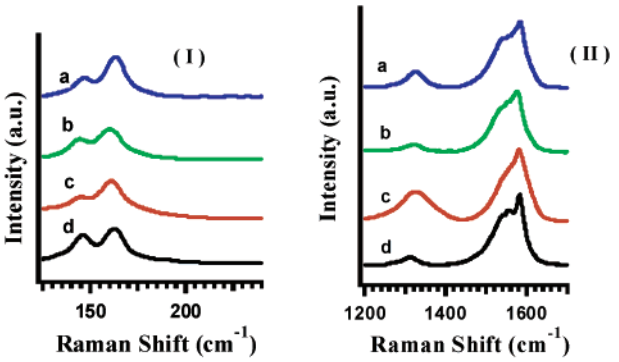

Figure 8. Raman spectroscopy data taken at 633 nm: (I) radial breathing modes; (II) tangential G (~1590 cm^{-1}) and disorder D (~1290−1320 cm^{-1}) band region. Top to bottom: (a) La^{3+}−SWNT adducts obtained from the initial chloride salts (blue); (b) La^{3+}−SWNT adducts obtained from the initial nitrate salts (green); (c) shortened, oxidized SWNTs (red); and (d) as-prepared SWNTs (black).

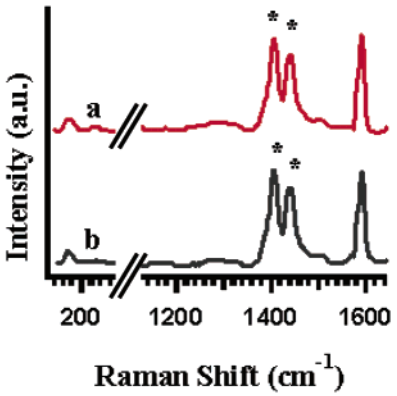

Figure 9. FT Raman spectroscopy data at 1064 nm. Top to bottom: (a) La^{3+}−SWNT adducts (red); (b) shortened oxidized SWNTs (black). (*) represents DMF solvent signals.

Figure 8 represents data of a dried, solid sample taken at 633 nm (1.96 eV), probing primarily a mixture of metallic and semiconducting tubes. From the RBM data in Figure 8I, at 633 nm excitation, the tube diameters are calculated to be 1.50 and 1.70 nm. We were able to obtain solution-phase results (Figure 9) only at 1064 nm excitation; interference from fluorescence in the dispersion prevented us from collecting spectra at lower excitation wavelengths. The corresponding RBM results calculated from these FT Raman data show that the tubes have a diameter of ~1.42 nm. It is worth noting that the laser excitation at 1064 nm (1.17 eV) will probe primarily semiconducting tubes.[56,57] In both cases, the range of tube diameters we have obtained does not fully represent the full diameter distribution of tubes present in this sample.

In general, there were no significant changes observed in the Raman spectra among raw, purified, and functionalized tubes. For instance, there were no significant changes in the position of the RBM peak in the oxidized SWNTs relative to that of the raw tubes (Figure 8I). In addition, the ratios of the RBM intensities for the functionalized SWNT adducts are more similar to those

(48) Zhang, J.; Wang, G.; Shon, Y.-S.; Zhou, O.; Superfine, R.; Murray, R. W. *J. Phys. Chem. B* **2003**, *107*, 3726.
(49) Brittan, H. G.; Wayda, A. L. *Inorg. Chim. Acta* **1984**, *95*, L1.
(50) Dresselhaus, M. S.; Dressehaus, G.; Jorio, A.; Souza Filho, A. G.; Saito, R. *Carbon* **2002**, *40*, 2043.
(51) Yu, Z.; Brus, L. E. *J. Phys. Chem. B* **2001**, *105*, 6831.
(52) Rao, A. M.; Richter, E.; Bandow, S.; Chase, B.; Eklund, P. C.; Williams, K. A.; Fang, S.; Subbaswamy, K. R.; Menon, M.; Thess, A.; Smalley, R. E.; Dresselhaus, G.; Dresselhaus, M. S. *Science* **1997**, *275*, 187.
(53) Corio, P.; Brown, S. D. M.; Marucci, A.; Pimenta, M. A.; Kneipp, K.; Dresselhaus, G.; Dresselhaus, M. S. *Phys. Rev. B* **2000**, *61*, 13202.
(54) Bahr, J.; Tour, J. M. *J. Mater. Chem.* **2002**, *12*, 1952.
(55) Holzinger, M.; Abraham, J.; Whelan, P.; Graupner, R.; Ley, L.; Hennrich, F.; Kappes, M.; Hirsch, A. *J. Am. Chem. Soc.* **2003**, *125*, 8566.
(56) Alvarez, L.; Righi, A.; Guillard, T.; Rols, S.; Anglaret, E.; Laplaze, D.; Sauvignol, J.-L. *Chem. Phys. Lett.* **2000**, *316*, 186.
(57) Kataura, H.; Kumazawa, Y.; Mainwa, Y.; Umezu, I.; Ohtsuka, Y.; Achiba, Y. *Synth. Met.* **1999**, *103*, 2555.

of the oxidized SWNTs than those of the raw tubes. However, in comparing the as-prepared SWNTs with the oxidized SWNTs, there were differences noted in the actual intensity of the peaks. For example, there was a relatively noticeable decrease in intensity of the lowest energy band at ~146 cm^{-1} for the oxidized tubes as compared with that of the raw tubes in the RBM intensity. This implies that oxidation affected the larger-diameter SWNTs to a greater extent than the smaller-diameter tubes. One plausible explanation for this observation can be attributed to a differential coupling of the electronic resonance enhanced spectra to the laser excitation wavelength energy, as opposed to an intrinsic change in tube diameter populations in the oxidized sample.[55] Another credible explanation for the attenuation of signal at 146 cm^{-1} is that larger-diameter tubes are more susceptible to acid intercalation[58] during the oxidation step, and hence, under these conditions, would have their resonances suppressed. These resonances recover to some extent upon functionalization, which likely involves a corresponding deintercalation process involving the tubes as coordination of the metal ions to the nanotubes happens.

As noted in Figure 8II, there is an increase in the I_D/I_G ratio (with I_D and I_G representing the intensities of the disorder and tangential modes at 1290−1320 and 1590 cm^{-1}, respectively) for the oxidized SWNTs as compared with the raw, as-prepared tubes, indicative of oxidative functionalization. This initial increase in the I_D/I_G ratio upon purification can be attributed to an increase of defect sites and in defect site distributions on the nanotube lattice due to oxidation and shortening of the SWNTs.[37,38] These defects include the conversion of sp^2-hybridized carbon to sp^3-hybridized carbon during the oxygenation process, with the creation of carboxylic acid and hydroxyl groups. Significantly, the I_D/I_G ratio subsequently decreases upon formation of the metal-functionalized adduct. This observed decrease of the I_D/I_G ratio upon lanthanide metal complexation can also be attributed to acid deintercalation from the nanotube tube bundles.[58]

In fact, tube oxidation and functionalization with the lanthanide ions has also significantly affected the G band of the metallic tubes, as compared with the raw tubes. The as-prepared SWNTs showed a slightly broad asymmetric band with a Breit−Wigner−Fano (BWF) profile, associated with metallic tubes. The BWF asymmetric shape is due to the coupling of phonons and electrons in metallic tubes.[51] This feature became less pronounced upon oxidation. However, upon functionalization with the lanthanide metal complexes, at 633 nm excitation, the BWF profile, indicative of the presence of metallic tubes, in the adduct spectrum was recovered and restored. Whereas charge transfer between nanotubes and attached metal complexes cannot be wholly ruled out,[24,59] a plausible physical explanation for the spectroscopic observation in this work resides in (a) the intercalation[60] of nitric acid into the tube bundles in the initial oxidation step followed by (b) the subsequent disruption and exfoliation of this hydrogen bonded network of bundles by the intervening presence of the coordinating metal ions during the lanthanide derivatization process. This results in the restoration of nanotube electronic properties, including the G band profile.

Conclusions

Thus, from all of these data, it can be concluded that end and defect site functionalization of SWNTs with metal complexes through the oxygenated groups, which potentially generate charge transfer complexes, can account for the observed results. Electrostatic interactions, such as the ionic ones accounting for adduct formation in this work, are likely to be important in the construction of layer-by-layer assemblies.[61,62] Hydrogen bonding plays a role in stacking the initial oxidized bundles that then become disrupted and exfoliated upon lanthanide derivatization. That is, disruption of hydrogen bonding upon functionalization will be crucial as a necessary preliminary step and a precursor to nanotube bundle exfoliation and solubilization.[23,24] Our nanotube-based structure is distinctive from previously reported lanthanide−C_{60} clusters.[63] Nevertheless, we expect our results to have implications for the generation of nanotube analogues of fullerene-based ferromagnets,[64] imaging contrast agents,[65] and drug derivatives.[66] Moreover, lanthanide-functionalized tubes patterned into arrays may have relevance for the fabrication of nanometer-scale optoelectronic devices.[67]

Acknowledgment. We acknowledge support of this work through startup funds provided by the State University of New York at Stony Brook as well as Brookhaven National Laboratory. Acknowledgment is also made to the National Science Foundation for a CAREER award (DMR-0348239) and to the donors of the Petroleum Research Fund, administered by the American Chemical Society, for support of this research. S.S.W. thanks 3M for a nontenured faculty award. We also thank Dr. James Quinn (Materials Science, SUNY at Stony Brook) for his help with the TEM analyses. The assistance of Dr. Alasdair Bell and Professor Peter Tonge with Raman analyses is much appreciated. Dr. Arthur Sedlacek (BNL) is thanked for his help with solution-phase FT-Raman work.

CM0349147

(58) Kukovecz, A.; Pichler, T.; Pfeiffer, R.; Kuzmany, H. *Chem. Commun.* **2002**, 1730.
(59) Menon, M.; Andriotis, A. N.; Froudakis, G. E. *Chem. Phys. Lett.* **2000**, *320*, 425.
(60) Bower, C.; Kleinhammes, A.; Zhou, O. *Chem. Phys. Lett.* **1998**, *288*, 481.
(61) Rouse, J. H.; Lillehei, P. T. *Nano Lett.* **2003**, *3*, 59.
(62) Mamedov, A. A.; Kotov, N. A.; Prato, M.; Guldi, D. M.; Wicksted, J. P.; Hirsch, A. *Nat. Mater.* **2002**, *1*, 190.
(63) Nagao, S.; Negishi, Y.; Kato, A.; Nakamura, Y.; Nakajima, A.; Kaya, K. *J. Phys. Chem. A* **1999**, *103*, 8909.
(64) Margiolaki, I.; Margadonna, S.; Prassides, K.; Hansen, T.; Ishii, K.; Suematsu, H. *J. Am. Chem. Soc.* **2002**, *124*, 11288.
(65) Iezzi, E. B.; Duchamp, J. C.; Fletcher, K. R.; Glass, T. E.; Dorn, H. C. *Nano Lett.* **2002**, *2*, 1187.
(66) Wilson, L. J.; Cagle, D. W.; Thrash, T. P.; Kennel, S. J.; Mirzadeh, S.; Alford, J. M.; Ehrhardt, G. J. *Coord. Chem. Rev.* **1999**, *190−192*, 199.
(67) Dickey, E.; Grimes, C. A.; Jain, M. K.; Ong, K. G.; Qian, D.; Kichambare, P. D.; Andrews, R.; Jacques, D. *Appl. Phys. Lett.* **2001**, *79*, 4022.
(68) Han, W.-Q.; Zettl, A. *Nano Lett.* **2003**, *3*, 681.